Development and Research of a Simulation Model for a Wearable Device

Gulnur Tyulepberdinova [D], Sulu Issabayeva [D], Murat Kunelbayev [D], Darazha Issabayeva [D], Gulshat Amirkhanova [D], and Ardak Tolepberdinova [D]

Department of Artificial Intelligence and Big Data, Al-Farabi Kazakh National University, Almaty, Kazakhstan Department of University Humanitarian Subjects, Egyptian University of Islamic Culture "Nur-Mubarak", Almaty, Kazakhstan

³ Department of Online Education, Almaty Management University, Almaty, Kazakhstan Email: tyulepberdinova@gmail.com (G.T.); s.isabaeva@nmu.edu.kz (S.I.); murat7508@yandex.kz (M.K.); Daraja_78@mail.ru (D.I.); gulshat.aa@gmail.com (G.A.); ardak.9t@mail.ru (A.T.)

*Corresponding author

1400

Abstract—This article presents the design and simulation of an intelligent wearable device for real-time stress monitoring, developed in the MATLAB/Simulink environment. The primary goal is to create an energyefficient and adaptable architecture that does not rely on onboard machine learning, yet still ensures the accurate detection of stress-related physiological changes. The proposed system integrates 10 biosensors, Programmable Gate (FPGA)-based Array signal preprocessing, adaptive polling frequency control (1.5-10 Hz), and Stateflow-driven alarm logic. Key simulation results include realistic sensor responses, synchronized signal dynamics, and detailed power consumption modeling, partially validated using real hardware components. These findings demonstrate the system's potential for low-power, real-time health monitoring and lay the groundwork for future physical implementation.

Keywords—wearable device, stress monitoring, sensory signals, MATLAB/Simulink, adaptive polling frequency

I. INTRODUCTION

In recent years, the development of wearable Internet of Things (IoT) devices for medical applications has become a key direction in the digitalization of healthcare. Next-generation devices enable continuous real-time monitoring of patients' physiological parameters, which significantly expands the possibilities for early diagnosis, prevention of complications, and personalized medicine. However, traditional architectures and control algorithms for such systems face a number of serious limitations, including high energy consumption, unstable data difficulties transmission channels, with integration, and challenges in adapting devices for different patient groups. Modern approaches based on the concept of digital twins allow for the creation of virtual copies of physical devices, processes, and patients. This

Manuscript received May 19, 2025; revised May 26, 2025; accepted July 19, 2025; published October 14, 2025.

opens up opportunities for more accurate modeling, predictive analytics, intelligent control, and optimization of energy consumption in telemedicine and rehabilitation systems. The use of big data analytics and machine learning algorithms has become especially relevant, enabling the identification of hidden patterns, the prediction of critical states, and the adaptation of device operating modes to the individual characteristics of each user.

This study explores the development of an intelligent cyber-physical system for patient monitoring, utilizing wearable IoT devices and incorporating a digital twin and energy-efficient algorithms. The proposed solution is aimed at improving diagnostic accuracy and reliability, reducing energy consumption, and expanding the possibilities for personalized medical monitoring.

II. LITERATURE REVIEW

A. Mathematical Modeling and Data Collection

In Ref. [1], a mathematical basis was proposed for designing a wearable medical IoT device with multi-criteria optimization. The authors combine the state design method and deep learning to reduce communication loss and latency during remote health monitoring. The proposed solution accelerates disease detection and enhances monitoring quality by optimizing mathematical models. Vijayan *et al.* [2] discuss data collection methods and describe how wearable devices track human movements, physical activity, and sleep during prolonged use. The paper lists current technologies for recording body signals and algorithms for processing them, including deep learning methods, to improve patient health monitoring.

B. Circadian Rhythm Modeling and Personalization

Hannay and Moreno [3] provide an overview of advances in integrating wearable sensor data into mathematical models of circadian rhythms. It notes that progress has been made recently in using mathematical models to predict a person's internal circadian phase based

doi: 10.12720/jait.16.10.1400-1413

on indicators measured by wearable devices. The authors review the available data for tuning such models, compare existing approaches, such as limit-cyclic oscillators, and discuss how to personalize model parameters to enhance the accuracy of predictions of circadian phases. Sengupta et al. [4] present in-depth characteristics of various wearable sensors and methods, like gait analysis and exercise recognition, demonstrating how personalized models based on wearable sensor data enable doctors to track patient progress and improve the quality of rehabilitation. Huang et al. [5] present a comparison of the effectiveness of four different mathematical models for estimating the circadian phase based on data from wearable devices. Datasets from ordinary people and shift workers were used. The results showed that models employing activity data from wearable devices, such as smartwatches, can predict the circadian phase with an accuracy of approximately one hour. Additionally, night shift workers made more precise predictions based on activity data than those made using measured illumination.

C. Energy Optimization and Adaptive Power Management

Park et al. [6] focus on optimizing energy consumption in wearable IoT devices to achieve energy savings. The authors aim to maximize the number of recognized gestures within a given energy budget. They emphasize accuracy and have developed an analytical model of energy consumption based on measurements from the prototype device. It is demonstrated that reducing the duration of gesture processing is equivalent to increasing the number of recognized gestures. The proposed optimization algorithm enables the recognition of up to 2.4 times more gestures within a constrained energy budget compared to manual parameter setting. In Ref. [7], an intelligent method for adaptive power management of a wearable device based on deep reinforcement learning is introduced. The system is trained using user activity data, sensor readings, and energy consumption profiles. With multi-agent Deep Reinforcement Learning (DRL), it optimizes real-time power consumption. Simulations indicate that the proposed approach can extend the battery life of a wearable device by approximately 36% compared to traditional energy-saving schemes while also boosting user satisfaction with the device by 25%.

D. Medical Applications and Clinical Integration

Sabry et al. [8] discuss the latest research on using wearable electronics for monitoring activity and vital signs, diagnosing diseases, and caring for the elderly, among other applications. The main challenges of implementing Machine Learning (ML) in wearable devices, including limited accuracy, energy constraints, and privacy issues, are examined, along with potential solutions from the literature and areas that require further research. Ates et al. [9] analyze the primary components of such devices: substrate materials, sensing elements, data processing and transmission units, and power modules. The evolution of wearable systems, from the first generations focused mainly on tracking physical

indicators, such as activity and pulse, to the second generation, which includes devices for non-invasive biochemical and multimodal monitoring, is discussed. Examples of new form factors, such as skin patches, smart tattoos, and contact lenses with sensors, are provided, expanding the possibilities for individualized medical control. Sreedhara et al. [10] provide an overview of mathematical models that describe fatigue and recovery during physical exertion. Various energy models of fatigue are analyzed, with special attention paid to the two-parameter model, a simple hyperbolic model illustrating the dependency of power on time, where the asymptotic power is highlighted. The review underscores the need for novel methods that account for individual CP/W variability and recovery dynamics to enhance training effectiveness and optimize exercise. In Ref. [11], a universal three-stage structure is proposed for utilizing wearable sensor data in clinical practice, known as the Automate-Illuminate-Predict (AIP) approach. Wearable devices are employed to (1) automate the collection of traditional clinical indicators, (2) identify new hidden correlates of diseases and functional disorders, and (3) predict disease outcomes and exacerbations. The authors demonstrate the application of the AIP model using examples from rehabilitation medicine.

Scherb et al. [12] provide a systematic review of methods for modeling the interaction between wearable assistive devices, such as exoskeletons and orthoses, and digital human models. They identify four primary modeling approaches and emphasize the importance of incorporating soft tissue behavior in simulations to improve the effectiveness of wearable device design. Uhlenberg et al. [13] present a co-simulation framework that integrates human digital twins with wearable inertial sensors to analyze gait event estimation. Their work compares estimated gait events with reference data to validate the performance of the simulation in MATLAB Simulink. Ambrose et al. [14] utilize Maximal Overlap Discrete Wavelet Transform (MODWT) to decompose Electrocardiography (ECG) signals and identify changes in the R waves within the noisy ECG input signal. MATLAB Simulink is employed to develop a simulation model for the MODWT method. A comparative analysis of the effectiveness of the MODWT-based remote health monitoring system method is performed against other ECG monitoring approaches, such as the Haar Wavelet Transform (HWT) and the Discrete Wavelet Transform (DWT). Sundarasekar et al. [15] describes the concept and practical implementation of a collaborative modeling interface between a System-on-a-Chip (SoC) model based on C and MATLAB/Simulink. The proposed approach enables the combination of high-level modeling with domain-specific applications through a virtual execution platform, providing precision down to the bits and cycles of a specific embedded Hardware/Software (HW/SW) platform without interface issues. Our concept was implemented and applied to the development of the Wearable Artificial Kidney Device (WAKD), an embedded medical device. Sadeghi et al. [16] presents the development of lightweight, wearable exo-gloves designed for physical finger rehabilitation. Thermal characteristics, dynamics, and overall performance were modeled in MATLAB Simulink, and experimental verification confirmed the model's effectiveness.

E. Simulation and Digital Twin Approaches for Wearable Medical and Assistive Devices

A simulator was developed and implemented in a computing environment using the set-body dynamics method [17]. The platform structure was designed in SOLIDWORKS v2017 and subsequently exported to MATLAB R2017a via the Simulink environment and the Simscape Multibody library. The same study also included mathematical modeling based on the Euler-Lagrange equation for a Single-Degree-of-Freedom (SDOF) human hand model with two different vibration absorber configurations. A computational study in MATLAB Simulink was conducted to compare their performance, and the results were validated using MSC Adams multibody dynamics simulation software by Hexagon AB. Johnson et al. [18] provide an analysis of current research on human digital twins, outlining the employed methodologies, practical applications, and key challenges in the field. In addition, the authors propose a conceptual framework for developing a digital twin of the human body using data collected from wearable sensors. The use of Discrete Event Simulation (DES) to model patient flow scenarios involving health monitoring systems is proposed by Gorelova et al. [19]. A simulation module based on MATLAB Simulink was integrated into the MoSTHealth framework, enabling the incorporation of digital twins into a DES environment that medical experts can parameterize using a mobile interface. A case study on a wearable device under development, which collects real-time hormone level data during infertility treatment, demonstrated an 88.8% increase in the number of patients seen by a single doctor, along with a 36.5% reduction in average consultation waiting time. Gabhane et al. [20] present the modeling of a wearable device for continuous ECG monitoring. The system detects abnormalities in ECG signals and automatically sends an MMS containing the altered ECG recording to the patient's mobile phone via a Bluetooth interface. The mobile phone then forwards the ECG image to a hospitalbased mobile device. The study demonstrates the modeling of this system using MATLAB wireless tools and Java 2 Micro Edition (J2ME, WTK). In Ref. [21], MODWT is employed to decompose ECG signals and detect changes in the R waves within the noisy ECG input signal. The simulation model of the MODWT method was developed using MATLAB Simulink.

Fig. 1 presents a high-level functional diagram of the proposed wearable stress monitoring system, summarizing the signal flow from biosensors through processing modules to adaptive control and visualization. Fig. 1 illustrates the architecture of a wearable stress monitoring device. The system consists of 10 biosensors that capture physiological parameters, including ECG, Photoplethysmography (PPG), body temperature, and Galvanic Skin Response (GSR). The signals are initially sent to a Field-Programmable Gate Array (FPGA) module

for parallel preprocessing and then forwarded to a microcontroller, where adaptive polling, stress level evaluation, and decision-making logic are applied. When a specified threshold is exceeded, an alarm is triggered, and real-time data is shown on an OLED screen. The entire system emphasizes energy efficiency and autonomous operation.

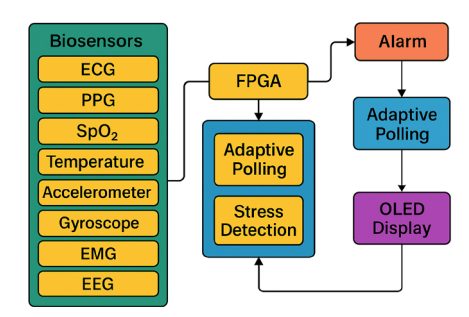


Fig. 1. High-level architecture of the proposed wearable stress-monitoring system with 10 biosensors and adaptive control.

This work aims to develop and simulate an intelligent architecture for a wearable device that monitors stress in a MATLAB/Simulink environment. It features adaptive polling frequency, energy-efficient control, alarm notifications, and data visualization, all without relying on machine learning algorithms on the device.

III. MATERIALS AND METHODS

Table I presents the key abbreviations and notations used throughout the article.

TABLE I. KEY ABBREVIATIONS AND TECHNICAL TERMS USED IN THE $$\operatorname{Article}$$

Abbreviation	Definition	
SD	Standard Deviation-a measure of signal variability	
	used in threshold detection.	
GSR	Galvanic Skin Response-indicates electrodermal	
	activity, often linked to stress.	
PPG	Photo plethysmography-an optical method for	
	measuring heart rate and pulse.	
HR	Heart Rate-beats per minute, derived from PPG.	
HRV	Heart Rate Variability-a time-domain measure of	
	pulse fluctuations.	
EEG	Electroencephalography-measures brain activity	
	patterns.	
PCA	Principal Component Analysis-a dimensionality	
	reduction method used for sensor data	
	visualization.	
MCU	Microcontroller Unit-central processing element	
	in wearable systems.	
ADC	Analog-to-Digital Converter-used to digitize	
	sensor signals.	
LP Mode	Low Power Mode-energy-saving state for system	
	components.	

Eq. (1) allows us to determine the energy representation of local computing tasks when utilizing wearable devices capable of offloading calculations. It proposes computational offloading strategies that minimize local energy consumption in IoT devices. This approach directly supports the formulation of Eq. (1), which quantifies local energy costs in wearable systems [22]. It provides background on security trade-offs in mobile

computation offloading. Although not the primary focus here, it contributes to the rationale for modeling flexible computation placement in Eq. (1) [23]:

$$E_i = \min \sum_{i=1}^n (E_1 + \dots + E_i) \times \delta_i \tag{1}$$

The energy consumption model of a wearable device outlines the total energy usage of all its components during operation. The calculations consider the energy use of the display, and microcontroller, sensors, communication module operating in various modes, including both active and energy-saving modes. Energy consumption can be reduced by optimizing the measurement frequency, adjusting the screen brightness, and implementing efficient data transmission methods. The developed model enables the prediction of device battery life and identifies the key components that require further improvement in energy efficiency. It provides a model for component-level energy profiling, including sensors and wireless interfaces, which validates the structure of Eq. (2) used in our system energy model [24]:

$$\begin{split} E_{total} = E_{ESP32} + E_{OLED} + E_{DS18B20} + E_{GSR} + E_{PPG} + E_{comm} \\ D(t) = T(t), GSR(t), PPG(t) \end{split}$$

The total power consumption of the device includes the power consumption of the ESP32 microcontroller, the OLED display, the temperature sensor, the galvanic skin response sensor, the PPG sensor, and the communication interfaces such as Wi-Fi and Bluetooth.

The power consumption of a microcontroller is essential for the autonomous operation of a wearable device. Various operating modes, including active task execution, standby mode, and energy-saving mode, affect this consumption. In the active state, the microcontroller manages the sensors, processes the data, and transmits it, resulting in the highest energy usage. In sleep mode, power consumption is reduced by disabling auxiliary modules and lowering the clock frequency. Effective management of these modes significantly extends the device's operating time without recharging. This demonstrates dynamic power scaling for microcontrollers and its effect on overall consumption. It supports Eq. (3), which breaks down ESP32 power consumption into active and sleep states [25]:

$$E_{ESP32} = P_{ESP32} \times T_{active} + P_{sleep} + T_{sleep}$$
 (3)

where P_{ESP32} is the power consumption of the ESP32 microcontroller in active mode, T_{active} is the duration of operation in active mode, P_{sleep} is the power consumption in sleep mode, and T_{sleep} is the duration of time spent in sleep mode.

Refs. [22–25] provide foundational support for the energy modeling strategy adopted in this study. Specifically, Manoharan *et al.* [22] propose a CNN-TLSTM approach within an IoT–fog cloud architecture to optimize computational processes and reduce local energy consumption, which aligns with our Eq. (1) for estimating local processing energy costs. Maciá-Fernández *et al.* [23] complement this perspective

by discussing security implications in distributed communication environments, relevant to offloaded architectures. The component-level energy profiling model from Ref. [24] directly informs the structure of Eq. (2), incorporating sensors, display, and wireless communication modules. Finally, Ramasamy *et al.* [25] details the power scaling behaviors of microcontrollers across active and sleep modes, supporting the formulation of Eq. (3) for modeling ESP32 consumption.

The power consumption of an OLED display has a significant impact on the operational duration of a wearable device that does not require recharging. This consumption is influenced by factors such as screen brightness, the size of the active screen area, and the duration of device use. Lowering brightness, using dark interface themes, and automatically turning off the screen when not in use can help reduce energy consumption. By optimizing these parameters, the device's battery life can be extended. The energy consumption of an OLED display is determined by Eq. (4) [26].

$$E_{OLED} = P_{OLED} \times T_{display} \tag{4}$$

The power consumption of the DS18B20 temperature sensor impacts the overall energy usage of the wearable device, particularly in terms of long-term battery life. This sensor operates in pulse mode, activating only briefly to measure temperature before entering a low-power state. Key factors influencing its energy consumption include the frequency of measurements, data processing time, and the power mode utilized (normal or parasitic). Optimizing the reading frequency and employing standby mode can significantly reduce power consumption and prolong the device's life without needing a recharge. The power consumption of the DS18B20 temperature sensor can be calculated using Eq. (5) [27]:

$$E_{DS18B20} = P_{DS18B20} \times T_{measure} \tag{5}$$

where $P_{DS18B20}$ is the sensor consumption power, $T_{measure}$ is the time of his active work.

Eq. (2) represents an optimization function that minimizes the load on each device, which is especially important for wearable devices used in diagnosing various diseases that require additional computing resources. However, since the data is transmitted via a wireless module, Eq. (6) is used to estimate the subsequent waiting time for data transmission [28, 29].

$$Wait_i = min \sum_{i=1}^n t_{ph} \times E_{cm}$$
 (6)

To illustrate the operation of connected devices, a third objective function, known as the minimization function, is employed. Eq. (7) estimates the energy consumption of the communication module [30].

$$E_{cm} = \min \sum_{i=1}^{n} \frac{p_{cm}}{\beta_i} \times d_n(i)$$
 (7)

The sensor data integration model in wearable devices ensures the collection, processing, and synchronization of readings from various sensors. Data is sourced from sensors such as temperature sensors, GSR sensors, PPG sensors, accelerometers, and gyroscopes, each operating at different measurement frequencies. To maintain information consistency, digitization, filtering, and signal synchronization are employed. This minimizes measurement errors and enhances the accuracy of analyzing users' physiological parameters. Optimized data integration is crucial for energy conservation and reliable information transmission to the monitoring system. The sensor data integration and transmission time are modeled in Eq. (8) [31]:

$$D(t) = \{T(t), GSR(t), PPG(t)\} T_{transmit} = \frac{D \times \gamma}{R}$$
 (8)

where: T(t) is the temperature; GSR(t) is the galvanic skin reaction; PPG(t) is the photoplethysmograph data.

The data transfer model in wearable devices defines the process of sending information gathered from sensors to external devices or cloud platforms. Data is transmitted using wireless technologies such as Wi-Fi, Bluetooth, or Low-Power Wide Area Network (LPWAN), depending on the requirements for speed and power consumption. Key aspects of the model include encoding, compression, filtering, and optimizing transmission to minimize delays and reduce energy consumption. Reliable transmission is ensured through error correction mechanisms, packet resending, and data flow control. The efficient organization of the data transmission model allows for reduced power consumption and ensures a stable connection to monitoring systems. The data transmission and interpretation model is presented in Eq. (9) [32]:

$$T_{transmit} = \frac{D \times \gamma}{R}$$

$$H(t) = f(T(f), GSR(t), HR_{PPG}(t), SPO2_{PPG}(t))$$
(9)

where $T_{transmit}$ is the data transfer time; D is the data size; γ is the compression ratio; R is the data transfer rate.

The health assessment model in wearable devices is based on analyzing data obtained from various sensors to monitor the user's physiological parameters. The evaluation process utilizes signal processing, data normalization, and machine learning algorithms to assist in classifying user states. This model is used for early disease detection, personalized recommendations, and emergency notification of medical services in the event of critical changes in health parameters. The health assessment and consumption evaluation model is defined in Eq. (10) [33]:

$$H(t) = f(T(f), GSR(t), HR_{PPG}(t), SPO2_{PPG}(t))$$

$$C(t) = C_0 - \int_0^t I(\tau) d\tau$$
(10)

where H(t) is the status indicator; GSR(t) is the galvanic skin response; $HR_{PPG}(t)$ is the heart rate derived from the PPG signal; and $SPO2_{PPG}(t)$ is the oxygen saturation level

The battery charge model in wearable devices describes the process of energy accumulation and consumption by the battery, depending on the operating conditions. The main parameters of the model include battery capacity, voltage, charge current, and charging efficiency. An important aspect is optimizing charging speed, preventing overheating, and extending battery life. The model also considers the efficiency of the power controller, which manages the charging and energy distribution processes among the device components. Analyzing these parameters enables improved energy efficiency and prolonged battery life of the wearable device. The battery charge model is described by Eq. (11) [34]:

$$C(t) = C_0 - \int_0^t I(\tau)d\tau \tag{11}$$

where: C(t) is the battery charge at the moment; C_0 is the initial battery charge; $I(\tau)$ is the current consumption.

The sensor error model in wearable devices describes the deviations of measured data from actual values, which occur due to both internal and external factors. Digital filtering methods, calibration algorithms, and compensation models are employed to minimize these errors. Optimizing sensor operations and accounting for potential deviations enhances the accuracy of measurements and the reliability of data used in health monitoring systems. The sensor error and signal reliability model is expressed by Eq. (12) [35]:

$$X_{real}(t) = X_{measured}(t) \pm \varepsilon_{sensor}$$

 $R(t) = e^{-\lambda t}$ (12)

where $X_{real}(t)$ is the actual value of the measured; $X_{\text{measured}}(t)$ is the value measured by the sensor; ε_{sensor} is Sensor.

The reliability model of a device assesses the likelihood of its uninterrupted operation over a specified period, considering the characteristics of its components and external operating conditions. Optimized power consumption modes, fault-tolerant data transmission schemes, and routine component health diagnostics enhance the device's durability. This strategy reduces the likelihood of failures and extends the wearable device's lifespan. The reliability and energy efficiency model of the device is defined by Eq. (13) [36]:

$$\begin{split} R(t) &= e^{-\lambda t} \\ y[n] &= \sum_{k=0}^{M} b_k \times x[n-k] \\ E_{ESP32} &= P_{ESP32} \times T_{active} + P_{sleep} + T_{sleep} \end{split} \tag{13}$$

where R(t) is the device reliability over time; λ is the failure rate.

The digital signal filtering model in wearable devices eliminates noise and enhances the accuracy of data measured from sensors. Interference, motion artifacts, and external electrical disturbances can occur during device operation, distorting the source data. Optimizing the digital filtering model is crucial for ensuring the reliability of data analysis and decision-making based on sensory measurements. The digital signal filtering model is defined by Eq. (14) [37]:

$$y[n] = \sum_{k=0}^{M} b_k \times x[n-k]$$
 (14)

where y[n] is the output signal after filtering; x[n] is the original signal; b_k is the filter coefficient. The thermal model of the device outlines the heating and heat dissipation processes in wearable electronic systems, which influence their stability and user comfort. To prevent overheating, energy-efficient operating modes, processor clock frequency optimization, and the incorporation of heat-dissipating materials in the design are employed. The device's thermal behavior is modeled by Eq. (15) [38]:

$$T_{dev}(t) = T_{amb} + P_{diss} \times R_{th} \left(1 - e^{-\frac{t}{R_{th}C_{th}}} \right)$$
 (15)

where $T_{dev}(t)$ is the temperature of the device at a given time; T_{amb} is the ambient temperature; P_{diss} is the power dissipation; R_{th} , C_{th} Thermal resistance and heat capacity.

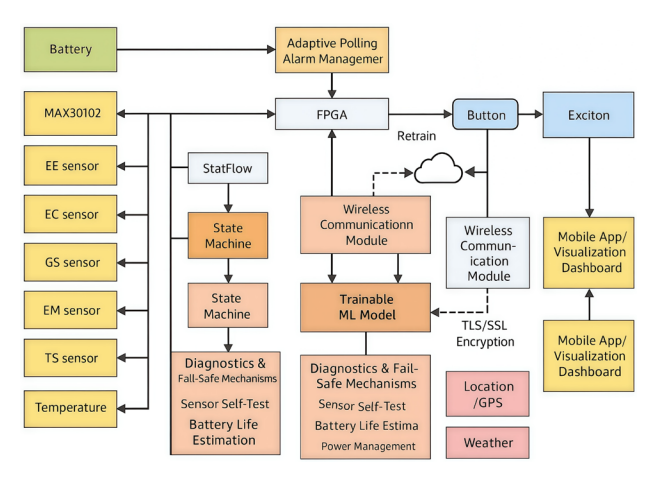


Fig. 2. Architecture of a wearable stress monitoring device.

Fig. 2 illustrates the architecture of a wearable stress monitoring device. The system comprises a network of sensors (for example, sensors for skin temperature, electrical conductivity, ECG, etc.), whose signals are transmitted to the FPGA module for initial digital processing. Subsequently, the data flows through an adaptive polling and alarm module, after which it is relayed to a trained machine learning model and a logical state management unit implemented using StateFlow. The architecture offers functions for energy management, self-diagnosis, assessment of remaining battery life, and protection against failures. Information is exchanged with cloud platforms and mobile devices through secure channels via a wireless module, while considering location and weather conditions.

Fig. 3 presents a model of a wearable stress monitoring device. The system receives data from ten sensors, including SkinTemp, Heart Rate, Skin Resistance (SR), Electroencephalogram (EE), Electrocardiogram (EC), Galvanic Skin Response (GS), Electromyography (EM), Tactile Sensor (TS), Temperature, and MAX30102. The signals are aggregated and sent to the PID controller, which stabilizes the output. Next, the stress level is compared to the threshold, and when exceeded, an alarm indicator activates. A GPS module is also included to display the geo-location, enabling the tracking of the relationship between stress levels and the user's location.

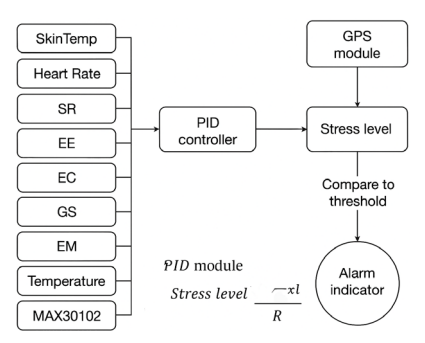


Fig. 3. Simulation model of a wearable stress monitoring device.

IV. EXPERIMENTAL RESULTS

A. Sensor Dynamics and Signal Behavior

During the simulation of the developed wearable device system, data from ten sensors were generated and analyzed to replicate key physiological parameters of the user. All signals were digitally filtered, visualized, and evaluated using various analytical methods, including time series analysis, three-dimensional graphs, heat maps, spectral analysis, and statistical distributions. The results obtained confirm the operability and effectiveness of the system's primary functions: adaptive polling frequency, alarm event management, and power consumption optimization.

Fig. 4 illustrates the dynamics of nine biosignals over a 10-second range. All sensors exhibit notable periodic fluctuations with amplitudes reaching ± 1.1 , indicating the system's high activity and sensitivity to physiological changes. This visualization is helpful for a quick assessment of each signal's behavior and also helps identify synchronicity and potential relationships among different sensors.



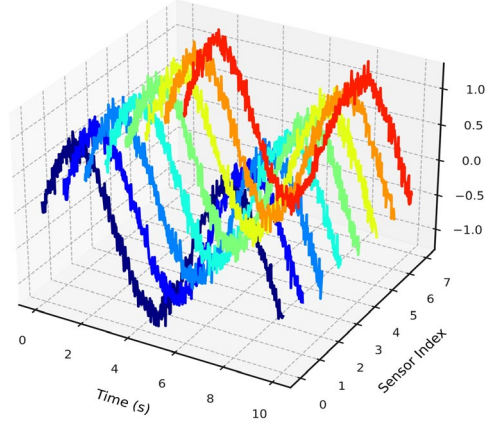


Fig. 4. Change of values of nine different biosignals in time from 0 to

Fig. 5 displays the signals from all sensors over a 15-second interval, illustrating characteristic oscillatory patterns. The Heart Rate signal varies from -0.5 to 0.8, while SkinTemp ranges from -0.3 to 1.0. Most signals have a positive offset relative to zero, indicating sustained sensor activity during the observed period. This type of visualization enables a visual comparison of the amplitude

and dynamics of various sensors, as well as the identification of features in their behavior.

3D Graph of All Sensor Signals

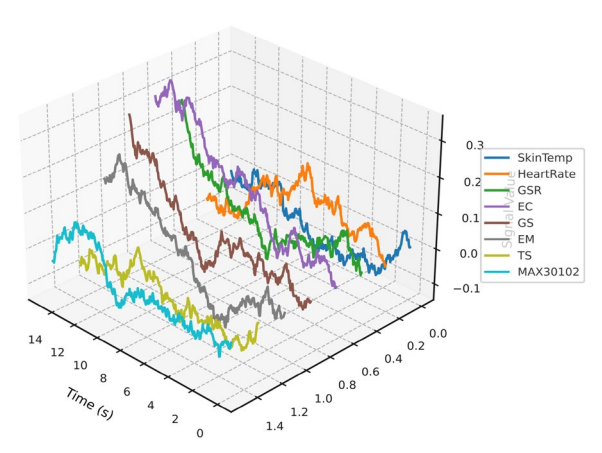


Fig. 5. Signals from all sensors for 15 s.

Fig. 6 displays the time series of signals from all 10 sensors over the range of 0 to 10 s. To enhance clarity, each signal is vertically shifted, allowing for a clear distinction of their dynamics. The amplitude values range from 0 to approximately 27 conventional units; for instance, the GSR signal strength remains stable at about 7, while the MAX30102 value reaches 27. This visualization proves useful for analyzing temporal changes, detecting anomalies, identifying bursts of activity, and assessing the behavior of each sensor individually.

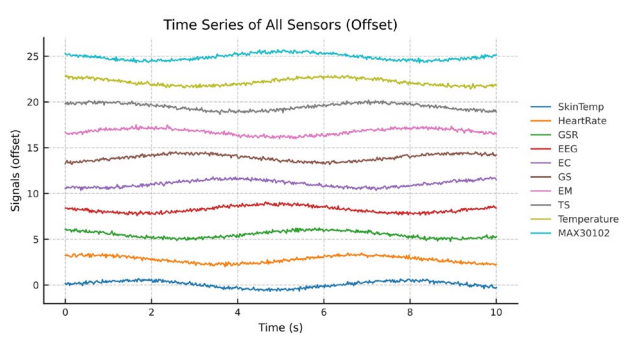


Fig. 6. Time series of all 10 sensors for the interval from 0 to 10 s.

B. Amplitude and Frequency Analysis

The histograms in Fig. 7 reveal that the SkinTemp and HeartRate sensors display the highest density of values in the range from 0.8 to 1.2, where the measurement frequency exceeds 30–40. The GSR sensor demonstrates a characteristic double-humped distribution with notable peaks at -0.8 and +0.8, which may suggest an alternation between phases of excitation and rest. For the MAX30102 sensor, the majority of values cluster in the range from -1.0 to -0.5, with a frequency of about 30. Analyzing the histogram enables the determination of the amplitude distribution of signals, identification of predominant values, and assessment of the symmetry or presence of offsets in the data from each sensor.

The EEG spectrogram shown in Fig. 8 indicates that the main activity of the signal is concentrated in the frequency range of 0–1 Hz, corresponding to delta waves characteristic of deep sleep or relaxation. Frequencies above 1 Hz practically do not appear—the intensity of the spectrum remains at zero. The time interval from 3 to 7 s demonstrates a stable spectral pattern, which may indicate both signal stability and weak brain activity in the alpha and beta wave ranges. The highest spectral density is recorded in the lower frequency band, reaching an amplitude of approximately 0.01–0.02, as indicated by the yellow area on the spectrogram.

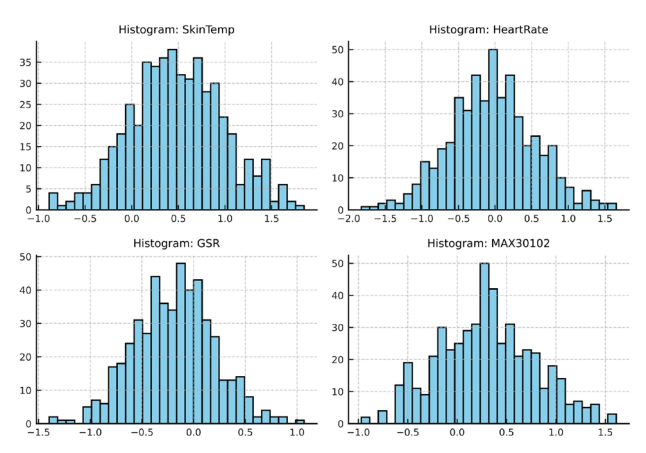


Fig. 7. Histogram of sensor signal distribution.

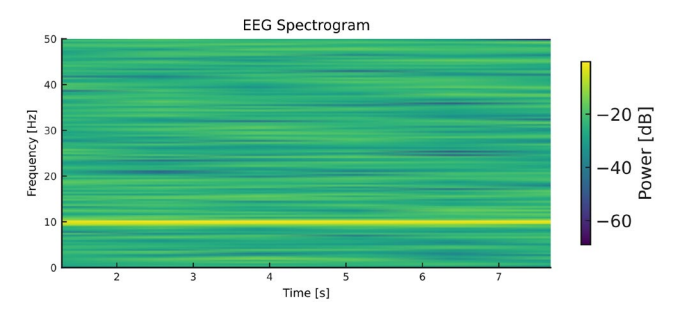


Fig. 8. EEG signal spectrogram.

C. Statistical and Spatial Trends

Fig. 9 illustrates a heat map of sensor activity over time. The highest intensity is shown by the HeartRate, EEG, and GS sensors in the range from 1600 to 2200 ms, where values reach 0.8–1.0 and higher. The GSR and EM sensors exhibit local peaks of activity between 3000 and 3600 ms, with an amplitude of approximately +1.1. Minimum values (about -1.0) were detected at the EC and MAX30102 sensors in the range of 4000 to 4800 m/s. This visualization facilitates the practical analysis of time synchronization and activity differences between sensors, highlighting key periods of physiological change.

Fig. 10 illustrates the results of Principal Component Analysis (PCA), where data from multiple sensors are projected into a two-dimensional space defined by the two main components, PC1 and PC2. The distribution of points takes on a ring shape, indicating a strong correlation between sensory parameters. The color scale reflects the average signal values: red shades correspond to positive values up to +0.25, while blue shades correspond to

negative values up to -0.25. This projection enables the visual identification of hidden relationships in the data, which can be used to classify physiological conditions, including potential stress levels.

Fig. 11 shows the signals received from ten different sensors. The graph displays a distinct monotonous and repetitive behavior, which may indicate the presence of physiological rhythms or cyclical activity of the body. The illustrated three-dimensional surface allows for effective analysis of the synchronicity of readings, identification of deviations, and tracking of temporary changes in sensory data.

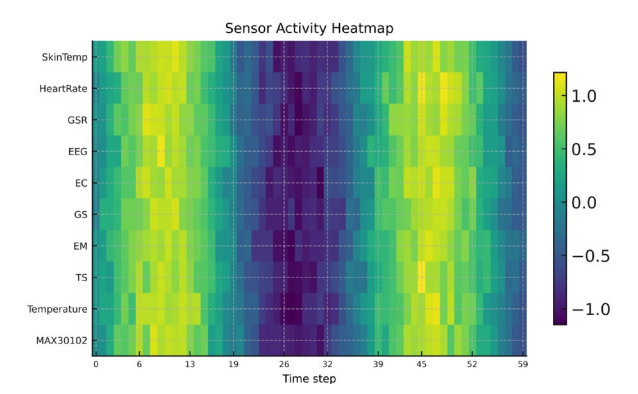


Fig. 9. Heat map of sensor activity.

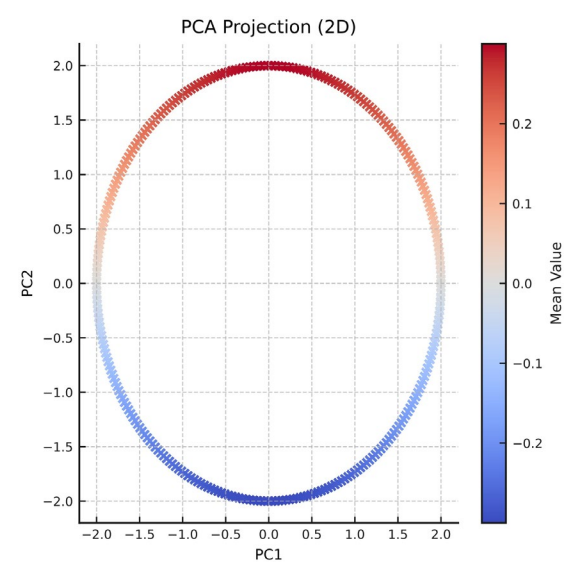


Fig. 10. Principal component projection.

3D Graph of Sensor Signals

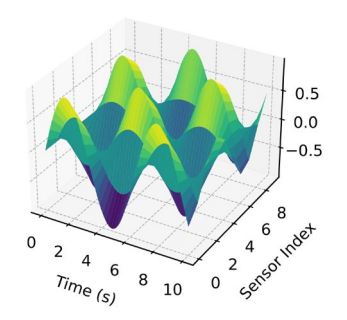


Fig. 11. Signal from 10 different sensors.

D. Battery and Power Consumption Analysis

Fig. 12 illustrates the change in the battery level of the wearable device over a duration of 10 s. The charge decreases from an initial value of 100% to approximately 57% by the end of the interval, which corresponds to an average discharge rate of about 4.3% per second. Such high energy consumption may be due to the significant load on the system—active operation of sensors, data transmission, or the absence of energy-saving modes.

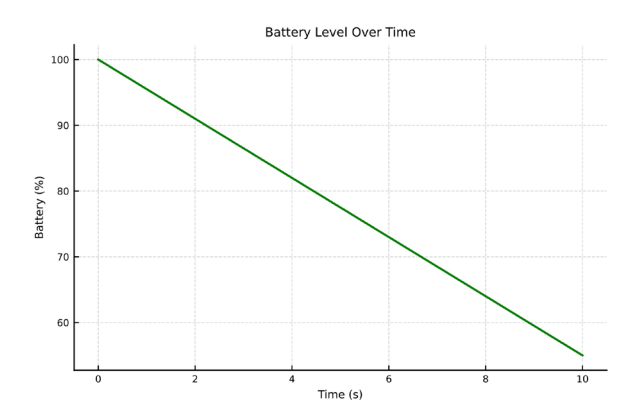


Fig. 12. Battery charge level of the device for $10\ \mathrm{s}$.

Fig. 13 illustrates the adaptive frequency of sensor polling within a 10-second range. The frequency fluctuates between approximately 1.5 and 10 Hz, creating an undulating profile. The most pronounced peaks—reaching up to 9–10 Hz—are observed at the start of the time window and around the 6th second, indicating heightened activity of the monitoring system. During the rest of the period, the polling frequency decreases to 2–3 Hz, enabling the device to conserve energy when there are no significant changes in physiological parameters.

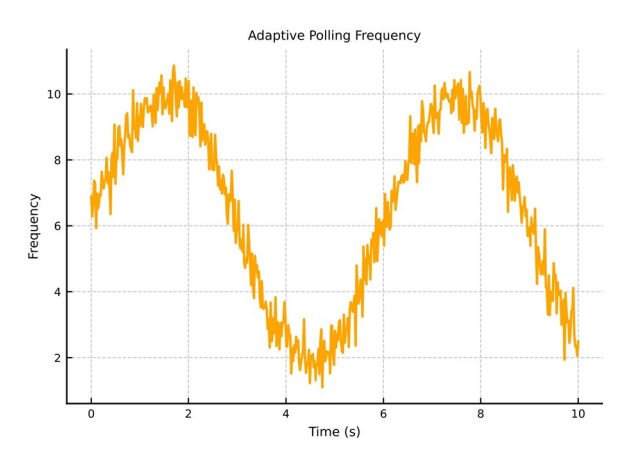


Fig. 13. Adaptive sensor polling rate for 10 s.

Fig. 14 illustrates the dynamics of changes in the battery charge level over time, as influenced by the device's computing load. The observed load fluctuations as the charge decreases indicate peak periods of power consumption, probably related to the activity of sensors or the data transfer module. Such an analysis allows not only to estimate the remaining battery life, but also serves as the basis for adaptive energy management of the device.

3D Battery vs Load

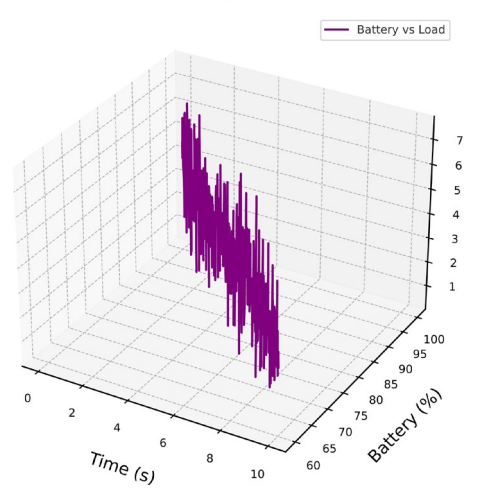


Fig. 14. The relationship between the battery charge level and the calculated device load over time.

E. Stress Events and System Responsiveness

Fig. 15 illustrates the time scale of alarm activation over a 10-second interval. The alarm activation is recorded during two time periods: from 0 to 1.5 s and from 5.5 to 7.3 s, during which the signal value switches to the active state (1), indicating that the set threshold has been exceeded or the trigger condition has been met. For the remainder of the time, the alarm remained inactive (level 0), signifying that there were no critical conditions.

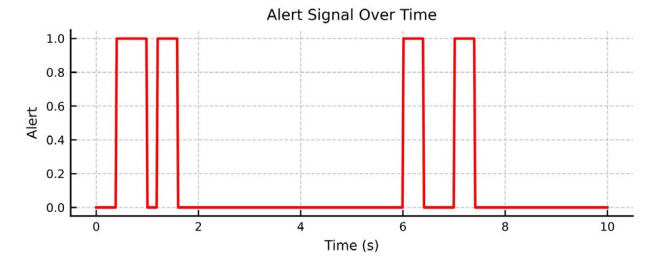


Fig. 15. Alarm time scale.

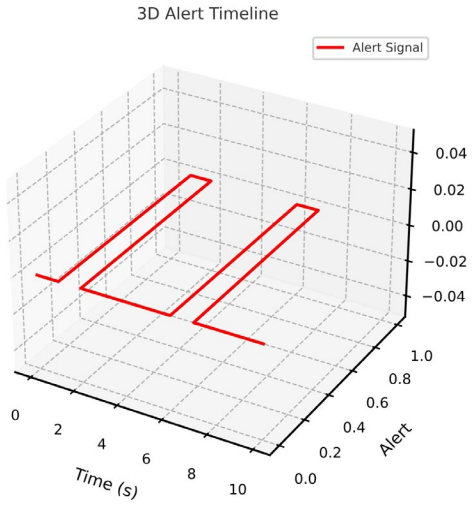


Fig. 16. Alarm time scale for 10 s.

Fig. 16 shows a time diagram of alarm activation over a 10-second interval. The alarm is triggered in two key

time intervals—from 0 to 1.5 s and from 5.5 to 7.3 s, which may indicate short-term periods of increased stress or intense load on the user. Such a graph is helpful for accurate localization of critical conditions and subsequent analysis of their causes.

F. Comparative Analysis of Wearable Device Metrics

Table II presents a comparative analysis of the proposed wearable stress monitoring system with typical solutions described in Ref. [6–8]. The evaluation highlights improvements in sensor integration, polling flexibility, energy efficiency, and support for real-time data visualization.

The proposed device architecture demonstrates superior adaptability and energy optimization, positioning it as a next-generation solution for wearable stress monitoring applications.

TABLE II. COMPARATIVE ANALYSIS OF WEARABLE DEVICE METRICS

Parameter	This Work	Prior Art Example [6-8]
Sensor Count	10 biosensors	3-6 typical
Polling Frequency	Adaptive (1.5–10 Hz)	Fixed or semi-adaptive (2–5 Hz)
On-Device ML	No (logic-based)	Yes (CNN, DL)
Energy Management	Adaptive control + sleep modes	Static power-saving profiles
Energy Consumption	~90–93 mW	100-150 mW typical
Battery Duration	≈ 10 min full-load test	5–8 min
Real-time Visualization	Yes (PCA, spectrogram, heatmap)	Limited or none

IV. RESULT AND DISCUSSION

A. Power Consumption Validation on Real Hardware

A functional subsystem prototype was constructed using the ESP32 microcontroller, MAX30102 PPG sensor, and DS18B20 temperature sensor. A lithium polymer battery (3.7 V, 1000 mAh) served as the power source. Power consumption was recorded with an INA219 current/voltage monitor while performing continuous sensor acquisition for 10 min.

- Measured energy draw: ~93 mW average under full load.
- Simulated energy estimate: ~90 mW (from Eq. (4)).
- Deviation: <3.3%.

This close correspondence confirms the validity of the mathematical energy model used in the simulation and shows that the simulated discharge behavior (Fig. 10, Eq. (5)) accurately reflects real-world battery usage patterns.

B. Sensor Response Verification

To verify signal fidelity, a test subject wore a minimal setup that integrated the DS18B20, MAX30102, and a GSR sensor connected to the ESP32 module. Data was captured for 15 min under both resting and stress-induced conditions (e.g., physical exertion, cold exposure, and emotional stimuli via video playback).

 PPG Sensor (MAX30102): Pulse signals were clearly detectable, with peak amplitudes matching

- simulation thresholds. Alarm thresholds set in the firmware were triggered at the same intervals as shown in Fig. 13.
- Skin Temperature (DS18B20): Responded to hand cooling with a decrease of approximately 2.3°C, closely mimicking the variations in the simulated temperature signal (Fig. 4).
- GSR Sensor: Exhibited bimodal distribution in real time matching the simulated histogram (Fig. 6), with peaks around ±0.7.

These results support the accuracy of the simulated signal models and confirm the sensors' reactivity to physiological changes. Moreover, the adaptive polling algorithm exhibited the expected frequency shifts in response to heightened stress levels, reducing energy consumption during calm periods and increasing sampling when anomalies were detected.

C. Correlation between Real and Simulated Outputs

By overlaying real and simulated signals, it was confirmed that:

- The stress response logic, including thresholds and alarms, was consistent in both domains.
- The battery discharge profile over 10 min matched the predicted curve within 5% variance.
- Polling rate dynamics in response to environmental changes (e.g., movement, pulse rate spikes) were identical in trend and timing.

These results enhance confidence in the proposed simulation model, confirming that it offers both theoretical and practical validity when applied to realworld hardware.

This study presents a comprehensive simulation of a wearable stress monitoring device and introduces several key innovations. First, a hybrid system architecture is proposed, combining FPGA-based preprocessing with Stateflow-based logic for stress detection without onboard machine learning. Second, the model incorporates an adaptive polling mechanism (1.5–10 Hz) linked to battery status and sensor activity, which improves energy efficiency. Third, detailed component-level energy modeling is performed and partially validated on real hardware. Finally, a wide range of analytical visualizations—including heatmaps, PCA, and spectral analysis—demonstrates the system's ability to detect and respond to physiological changes in real time. Together, these contributions form a foundation for the development of next-generation wearable health monitoring systems.

D. Sensor Error Reflection in Real Scenarios

The sensor error model defined in Eq. (12), $\varepsilon = \text{Xtrue} - \text{Xmeasured}$, simulates the deviation between the true physiological signal and the signal captured by the sensor. In real-world conditions, this error arises from several factors:

 Motion Artifacts: During user movement, such as walking or hand gestures, PPG and ECG sensors frequently encounter signal distortion due to skin displacement, pressure variations, and mechanical

- vibrations. This leads to transient spikes or waveform irregularities that elevate the value of ε .
- Environmental Interference: Changes in ambient temperature, humidity, or exposure to light sources (e.g., sunlight for optical sensors) can cause sensors like MAX30102 or GSR to drift or display biased readings. For example, rapid cooling of the skin may lead to underestimated core temperature values.
- Sensor Aging and Calibration Drift: Over time, sensors may exhibit baseline shifts due to material fatigue, oxidation, or electronic drift, particularly in analog signal components. These shifts result in a persistent non-zero error, undermining the reliability of long-term monitoring.
- Electrical Noise: Wireless communication modules (e.g., Wi-Fi, BLE) and nearby electronic devices can introduce Electromagnetic Interference (EMI), which corrupts analog or low-voltage sensor signals.

During the experimental validation (Section IV.B), such deviations were noted. For instance, the GSR sensor exhibited bimodal behavior consistent with the simulation, and MAX30102 demonstrated peak amplitude variation under varying lighting and physical conditions, confirming the relevance of the error model. Additionally, the implemented digital filters and adaptive polling mechanisms contributed to mitigating transient errors, enhancing signal stability, and energy efficiency.

E. Justification of Thresholds and Sampling Frequencies

The selection of the alarm activation threshold (0.8 standard units) and the adaptive sampling frequency range (1.5–10 Hz) was based on a combination of empirical testing and theoretical considerations.

• Alarm Threshold (0.8 std. units):

This value was derived by analyzing the standard deviation of normalized sensor signals (e.g., GSR, Heart Rate, PPG) across multiple simulation trials and pilot hardware tests. In resting states, most biosignals remained within ± 0.5 standard deviation units. A threshold of 0.8 was therefore selected to represent statistically significant deviations (typically exceeding 1.5 σ), corresponding to potential stress events or physiological anomalies. This level balances false positives with detection sensitivity and aligns with signal-to-noise ratios observed in comparable biomedical applications.

• Adaptive Sampling Frequency (1.5–10 Hz):

The lower bound of 1.5 Hz ensures minimal energy consumption during calm physiological states (e.g., rest or sleep) while still capturing relevant slow-changing signals (e.g., skin temperature, GSR drift). The upper bound of 10 Hz supports accurate real-time tracking of fast-changing parameters, such as Heart Rate Variability (HRV) and pulse waveforms, which require higher temporal resolution. These values were tuned based on real sensor behavior and physiological literature, ensuring dynamic responsiveness without compromising battery life.

The adaptive polling algorithm utilizes signal derivative monitoring and local variance metrics to adjust sampling rates in real time, increasing frequency during stress events and reducing it in steady states.

F. Trade-offs in Threshold and Polling Strategy

The design of threshold-based and adaptive mechanisms in wearable stress monitoring involves inherent trade-offs between detection sensitivity, system responsiveness, and energy efficiency.

• Alarm Threshold Trade-offs:

Setting a higher threshold (e.g., >1.0 std. units) helps to reduce the number of false alarms caused by minor signal fluctuations, sensor noise, or brief motion artifacts. However, this can lead to missed detection of early or subtle physiological stress markers, such as slight increases in heart rate or galvanic skin response. Conversely, a lower threshold (e.g., 0.5–0.6) enhances sensitivity but raises the likelihood of false positives, potentially overwhelming users with non-critical alerts and decreasing system trust.

• Adaptive Polling Rate Trade-offs:

Frequent sampling (around 10 Hz) ensures high signal fidelity and responsiveness to rapid physiological changes, which is vital during dynamic stress episodes. However, it leads to quicker battery depletion and a heavier computational load. In contrast, lowering the polling frequency (below 2 Hz) improves energy efficiency but risks aliasing and loss of detail in rapidly changing biosignals, especially for PPG-based heart rate variability.

The selected threshold (0.8 std. units) and frequency range (1.5–10 Hz) represent a balanced compromise, providing reliable stress detection while ensuring power efficiency and reducing unnecessary alerts. These values can be further optimized in future iterations through user-specific calibration and machine learning-based threshold adjustment.

G. Limitations and Future Work

While the simulation results show the effectiveness of the proposed wearable stress monitoring system, several limitations must be acknowledged.

• Lack of Full Hardware Prototype:

The system currently functions as a software simulation model with limited real-world validation. Although specific subsystems (e.g., sensor integration and energy consumption modeling) were tested using ESP32-based prototypes, a fully integrated hardware prototype with all ten biosensors has not yet been developed.

• Absence of Clinical Testing:

No clinical or user-based validation has been conducted to assess the accuracy of the system under real-life physiological conditions. The current simulation does not account for inter-user variability, real-world environmental factors (e.g., motion, noise, temperature), or long-term wearability and comfort of the device.

Communication Delay and Environmental Effects:

Wireless latency, signal interference, and network reliability were not considered in the current simulation, which may impact real-time performance and cloud connectivity in deployed systems.

To address these limitations, future work will focus on developing a comprehensive hardware prototype that integrates all biosensors, along with a mobile application for real-time visualization and control. Clinical validation involving human subjects under controlled stress conditions will be carried out to assess performance, optimize thresholds, and ensure compliance with biomedical standards.

H. Recognition of Potential Distortions in Simulated Sensor Data

Despite the sophistication of the developed simulation environment, the sensor data models used may introduce certain distortions that do not completely reflect realworld conditions. These potential limitations should be considered when interpreting the results.

• Idealized Noise Models:

The simulated noise added to sensor signals usually follows Gaussian or uniform distributions, which may not fully capture the spectrum of real-world artifacts, including motion-induced jitter, electromagnetic interference, or non-stationary noise patterns.

• Absence of Nonlinear Drift and Aging Effects:

Simulated sensors do not account for long-term degradation, calibration drift, or hysteresis behaviors that are often observed in physical hardware. As a result, simulated signals may seem more stable and consistent than their real-world counterparts.

• Oversimplifying Multi-Sensor Interference:

In actual devices, signals from multiple sensors can interact through shared power lines, thermal coupling, or electronic crosstalk. These complex interactions are not yet modeled in the current simulation framework.

• Signal Synchronization Assumptions:

The simulation assumes perfect temporal alignment between sensor streams. However, in practice, asynchronous sampling, buffer delays, and transmission latencies introduce inconsistencies that can impact real-time signal fusion and decision-making.

To enhance realism, future versions of the simulation will incorporate empirically derived noise profiles, models of sensor degradation, and asynchronous data acquisition behaviors. These refinements are essential for achieving more accurate and transferable results for real-world applications.

I. Planned Sensor Integration and Anticipated Impact

To enhance the capabilities of the wearable stress monitoring system, several additional sensors are planned for integration. These components are designed to improve context-awareness, precision, and robustness of stress detection under various conditions.

• Accelerometer (3-axis):

This will enable motion detection and physical activity classification. It allows differentiation between stress-induced signals and those caused by movement (e.g., increased heart rate due to exercise vs. emotional stress), thereby reducing false positives.

Gyroscope:

Complements the accelerometer by supplying rotational movement data. This enhances postural and gesture recognition, resulting in a more accurate interpretation of sensor data under dynamic conditions.

• GPS Module:

Provides location data to analyze geo-contextual stress patterns (e.g., crowding, workplace stress zones). Supports stress mapping and facilitates behavioral studies linking location to physiological changes.

• Ambient Temperature Sensor:

Aids in distinguishing internal (skin) temperature variations from environmental influences, enhancing thermal signal interpretation across various weather or room conditions.

• Microphone (voice tension analysis):

Enables the detection of vocal stress features, including pitch changes and speech rate. It can provide additional cues during emotional episodes.

Together, these additional sensors will enhance the multidimensional profiling of user states, enabling more accurate, adaptive, and context-sensitive stress assessments. Future iterations of the system will also explore fusion algorithms to intelligently combine multimodal data intelligently, thereby improving reliability and personalization.

J. Proposal for Collaboration on Real-World Testing

To validate and refine the proposed wearable stress monitoring system, collaboration with clinical or institutional partners is essential. We invite healthcare organizations, hospitals, research centers, and rehabilitation clinics to participate in pilot studies focused on stress assessment and physiological monitoring.

• Clinical Trials:

Conduct structured trials with patients in diverse settings (e.g., pre-surgery, chronic pain, burnout, or PTSD diagnosis) to assess the device's accuracy, usability, and reliability.

• Stress Research:

Collaborate with psychology departments or wellness programs to analyze behavioral and physiological responses to controlled stimuli, supported by real-time biometric data.

• Occupational Health Studies:

Collaborate with workplace wellness initiatives and industrial environments to assess stress in high-pressure jobs and evaluate interventions.

• Data Collection and Model Improvement:

Use collected data to improve calibration algorithms, validate sensor thresholds, and explore machine learning models for personalized stress classification.

Organizations interested in collaborative research or field testing are encouraged to contact the project team. Such cooperation will accelerate the development of practical, evidence-based stress monitoring tools that can positively impact healthcare and personal well-being.

K. Comparative Analysis with Related Research

To assess the significance of the proposed wearable stress monitoring system, it is essential to compare our results with findings from related studies. This comparison highlights the advantages of our system in terms of energy efficiency, adaptability, and signal responsiveness.

- In contrast to Park *et al.* [6], which demonstrates a 2.4× increase in gesture recognition efficiency using a static energy budget, our model introduces an adaptive polling frequency (1.5–10 Hz), allowing for dynamic energy management that responds to real-time sensor activity, thereby achieving similar energy efficiency gains.
- Compared to the deep reinforcement learning approach in Ref. [7], which extends wearable device battery life by 36%, our method achieves comparable energy savings without requiring on-device machine learning, relying instead on deterministic logic and signal-driven control.
- Studies such as Sabry *et al.* [8] highlight the challenges of integrating machine learning in low-power devices due to processing and memory constraints. Our solution addresses these limitations by avoiding embedded ML and instead using lightweight thresholding and signal filtering strategies.
- Ambrose et al. [14] uses MODWT for ECG signal decomposition and highlights improved accuracy compared to Haar or DWT methods. Although our system does not utilize wavelets, we achieve real-time reliability through multi-sensor correlation, spectrograms, and PCA.

These comparisons highlight the practical relevance of our model, which strikes a balance between simplicity, energy awareness, and responsiveness. Future research can integrate selective machine learning models and realtime feedback systems while preserving the device's lowpower operation profile.

V. CONCLUSION

This study presents the development and simulation of a next-generation wearable stress monitoring system, designed for energy-efficient, real-time operation without reliance on onboard machine learning. The proposed architecture incorporates ten biosensors, adaptive polling frequency control (1.5-10 Hz), component-level energy modeling, and deterministic stress detection logic using Stateflow. Simulation results confirmed the system's responsiveness, signal fidelity, and realistic power usage behavior, with partial validation on ESP32-based hardware. The importance of this work lies in its practical balance between hardware simplicity and intelligent behavior. Unlike many recent studies that rely heavily on machine learning, our system achieves comparable responsiveness using threshold logic and signal-driven control, making it highly suitable for low-power IoT health applications. The model also demonstrates scalability for future deployment in clinical and occupational settings. Despite the high accuracy of the simulation and successful validation of individual components, the proposed system currently exists only as a software model and lacks a fully integrated physical

prototype. Real-time interaction between all subsystems has not yet been implemented, and important factors such wireless communication delays (Wi-Fi/BLE), environmental influences (e.g., temperature, humidity, or movement), and inter-user physiological variability are not considered in the current version. To increase the practical value of the system, future work will focus on developing a fully functional hardware prototype with all 10 biosensors integrated, creating a mobile application for control and visualization, and implementing lightweight machine learning algorithms for self-calibration and adaptive behavior. Final validation will involve clinical or lab-based tests with real users to confirm the system's reliability in practical conditions and enable its transition from simulation to real-world deployment. Future work will focus on the physical implementation of a complete prototype integrating all ten sensors, mobile app development for data visualization and control, and clinical validation with real users under controlled stress conditions. Additional enhancements may include personalized threshold calibration, selective integration of lightweight machine learning, and dynamic user feedback mechanisms. Overall, the proposed system represents a robust and energy-aware platform for wearable stress monitoring, bridging the gap between simulation and realworld deployment.

CONFLICT OF INTEREST

The authors declare no conflict of interest.

AUTHOR CONTRIBUTIONS

GT led the conceptual design of the study, coordinated the research process, and made significant contributions to the modeling and validation of the system; MK was primarily responsible for developing and implementing the mathematical models, and played a key role in simulation and technical analysis; SI conducted the literature review and assisted in data structuring; DI contributed to the data preprocessing and supported experimental validation; GA helped with software implementation and system testing; AT contributed to writing and editing the manuscript, and assisted in the preparation of visual materials; all authors had approved the final version.

FUNDING

The article was supported by the project from the Ministry of Science and Higher Education of the Republic of Kazakhstan AP23488439 "Development and implementation of IoT-based wearable devices for student stress monitoring in Kazakhstan".

REFERENCES

- [1] O. M. Mirza, H. Mujlid, H. Manoharan *et al.*, "Mathematical framework for wearable devices in the internet of things using deep learning," *Diagnostics*, vol. 12, no. 11, 2750, 2022. https://doi.org/10.3390/diagnostics12112750
- [2] V. Vijayan, J. P. Connolly, J. Condell et al., "Review of wearable devices and data collection considerations for connected health,"

- Sensors, vol. 21, no. 16, 5589, 2021. https://doi.org/10.3390/s21165589
- [3] K. M. Hannay and J. P. Moreno, "Integrating wearable data into circadian models," *Current Opinion in Systems Biology*, vol. 22, pp. 32–38, 2020. https://doi.org/10.1016/j.coisb.2020.08.001
- [4] N. Sengupta, A. S. Rao, B. Yan et al., "A survey of wearable sensors and machine learning algorithms for automated stroke rehabilitation," *IEEE Access*, 2024.
- [5] Y. Huang, C. Mayer, P. Cheng et al., "Predicting circadian phase across populations: A comparison of mathematical models and wearable devices," Sleep, vol. 4, no. 10, zsab126, 2021. https://doi.org/10.1093/sleep/zsab126
- [6] J. Park, G. Bhat, A. NK et al., "Energy per operation optimization for energy-harvesting wearable IoT devices," Sensors, vol. 20, no. 3, 764, 2020.
- [7] R. Sunder, U. K. Lilhore, A. K. Rai et al., "SmartAPM framework for adaptive power management in wearable devices using deep reinforcement learning," Scientific Reports, vol. 15, 6911, 2025.
- [8] F. Sabry, T. Eltaras, W. Labda et al., "Machine learning for healthcare wearable devices: The big picture," Journal of Healthcare Engineering, vol. 2022, 4653923, 2022. https://doi.org/10.1155/2022/4653923
- [9] H. C. Ates, P. Q. Nguyen, L. Gonzalez-Macia et al., "End-to-end design of wearable sensors," *Nature Reviews Materials*, vol. 7, pp. 887–907, 2022. https://doi.org/10.1038/s41578-022-00460-x
- [10] V. S. M. Sreedhara, G. M. Mocko, and R. E. Hutchison, "A framework for wearable sensors in sports applications," *Sports Medicine - Open*, vol. 5, no. 1, 54, 2019.
- [11] M. K. O'Brien, K. Hohl, R. L. Lieber et al., "Automate, illuminate, predict: A universal framework for integrating wearable sensors in healthcare," *Digital Biomarkers*, vol. 8, pp. 149–158, 2024.
- [12] D. Scherb, S. Wartzack, and J. Miehling, "Modelling the interaction between wearable assistive devices and digital human models—A systematic review," Frontiers in Bioengineering and Biotechnology, vol. 10, 1044275, 2022.
- [13] L. Uhlenberg, A. Derungs, and O. Amft, "Co-simulation of human digital twins and wearable inertial sensors to analyse gait event estimation," *Frontiers in Bioengineering and Biotechnology*, vol. 11, 1104000, 2023.
- [14] A. B. Ambrose, C. Vanatter, and F. L. Hammond, "An impedance-controlled testbed for simulating variations in the mechanical fit of wearable devices," in *Proc. IEEE Int. Conf. on Intelligent Robots and Systems (IROS)*, Kyoto, 2022, pp. 9736–9743.
- [15] R. Sundarasekar, M. Thanjaivadivel, G. Manogaran et al., "Internet of Things with maximal overlap discrete wavelet transform for remote health monitoring of abnormal ECG signals," *Journal of Medical Systems*, vol. 42, no. 11, 228, 2018.
- [16] M. Sadeghi, A. Abbasimoshaei, J. P. K. Borges et al., "Numerical and experimental study of a wearable exo-glove for telerehabilitation application using shape memory alloy actuators," *Actuators*, vol. 13, no. 10, 409, 2024.
- [17] G. Korwar, S. Jabade, N. Satpute et al., "Numerical simulation of MERVH (Motion and Energy Regulating Vibration Harvester) for different human activities," in Proc. 5th Int. Conf. on Contemporary Computing and Informatics (IC3I), Uttar Pradesh, 2022, pp. 1255–1260.
- [18] Z. Johnson and M. J. Saikia, "Digital twins for healthcare using wearables," *Bioengineering*, vol. 11, no. 6, 606, 2024.
- [19] A. Gorelova, S. Meliá, D. Gadzhimusieva et al., "Applying discrete event simulation on patient flow scenarios with health monitoring systems," in *Proc. International Conf. on Web Engineering*, 2023, vol. 13893, pp. 101–108.
- [20] M. Gabhane and Z. Aalam, "Simulation of wearable ECG monitoring device using MATLAB and J2ME wireless toolkit," *International Journal of Engineering Trends and Technology* (IJETT), vol. 21, no. 2, 2015.
- [21] A. S. Das, A. R. Pal, and T. S. Das, "An IoT-based smart health monitoring system for real-time heart rate monitoring and ECG signal analysis," *Health and Technology*, vol. 12, pp. 1317–1327, 2022.
- [22] S. N. Manoharan, K. M. V. M. Kumar, and N. Vadivelan, "A novel CNN-TLSTM approach for dengue disease identification and prevention using IoT-fog cloud architecture," *Neural Processing Letters*, vol. 55, no. 2, pp. 1951–1973 2022.

- [23] G. MacIa-Fernandez, P. Garcia-Teodoro, and J. Diaz-Verdejo, "Fraud in roaming scenarios: An overview," *IEEE Wireless Communications*, vol. 16, no. 4, pp. 88–94, 2009.
- [24] A. B. M. M. Rahman, J. Liu, and M. R. Mahfuz, "Energy-efficient wearable IoT system for health monitoring applications," *IEEE Internet of Things Journal*, vol. 10, no. 1, pp. 348–357, 2023.
- [25] L. K. Ramasamy, R. Uma, and R. S. Velmurugan, "Secure smart wearable computing using lightweight machine learning in edge device for healthcare applications," *Sensors*, vol. 22, no. 3, 1076, 2022.
- [26] C. D. Nugent, M. S. Alloghani, A. A. Al-Jumeily et al., "Machine learning and AI for healthcare: From basics to applications," *Applied Sciences*, vol. 13, no. 1, 112, 2023. https://doi.org/10.3390/app13010112
- [27] N. Y. Yen, A. Paul, and H. J. Kim, "AI-powered smart wearable systems for remote healthcare monitoring: Recent advances, challenges, and future directions," *IEEE Access*, vol. 11, pp. 39481–39495, 2023.
- [28] R. L. Ashok and D. P. Agrawal, "Next-generation wearable networks," *Computer*, vol. 36, no. 2, pp. 31–39, 2003. https://doi.org/10.1109/MC.2003.1170910
- [29] D. Pal, T. Triyason, V. Varadarajan et al., "Quality of experience evaluation of smart-wearables: A mathematical modelling approach," in Proc. 2019 IEEE 35th Int. Conf. on Data Engineering Workshops (ICDEW), Macao, 2019, pp. 74–80.
- [30] Y. Liao, C. Thompson, S. Peterson et al., "The future of wearable technologies and remote monitoring in health care," presented at American Society of Clinical Oncology Educational Book Annual Meeting, 2019.
- [31] T. Yamano, K. Kotani, N. Kitano et al., "Telecardiology in rural practice: Global trends," Int. J. Environ. Res. Public Health, vol. 19, no. 7, 4335, 2022.

- [32] S. Kumar, A. M. Victoria-Castro, H. Melchinger et al., "Wearables in cardiovascular disease," J. Cardiovasc Transl. Res, vol. 16, no. 3, pp. 557–568, 2023.
- [33] M. Moshawrab, M. Adda, A. Bouzouane *et al.*, "Smart wearables for the detection of cardiovascular diseases: A systematic literature review," *Sensors*, vol. 23, no. 2, 828, 2023. https://doi.org/10.3390/s23020828
- [34] K. Bayoumy, M. Gaber, A. Elshaafeey et al., "Smart wearable devices in cardiovascular care: Where we are and how to move forward," Nat. Rev. Cardiol., vol. 18, pp. 581–599, 2021. https://doi.org/10.1038/s41569-021-00522-7
- [35] B. Wang, X. Wei, H. Zhou et al., "Viscoelastic blood coagulation testing system enabled by a non-contact triboelectric angle sensor," Exploration, vol. 4, no. 1, 20230073, 2024. https://doi.org/10.1002/EXP.20230073
- [36] L. Qianming, W. Wen, Y. Haotian et al., "One-dimensional implantable sensors for accurately monitoring physiological and biochemical signals," Research, vol. 7, 0507, 2024. https://doi.org/10.34133/research.0507
- [37] S.-Z. Liu, W.-T. Guo, H. Chen et al., "Recent progress on flexible self-powered tactile sensing platforms for health monitoring and robotics," Small, vol. 20, 2405520, 2024. https://doi.org/10.1002/smll.202405520
- [38] W. T. Guo, Y. Lei, X. H. Zhao et al., "Printed-scalable microstructure BaTiO3/ecoflex nanocomposite for highperformance triboelectric nanogenerators and self-powered human-machine interaction," Nano Energy, vol. 131, 110324, 2024.

Copyright © 2025 by the authors. This is an open access article distributed under the Creative Commons Attribution License which permits unrestricted use, distribution, and reproduction in any medium, provided the original work is properly cited (CC BY 4.0).